Dynamic Behavior of the Doubly Fed Induction Generator During Three-Phase Voltage Dips

Jesús López, *Member, IEEE*, Pablo Sanchis, *Member, IEEE*, Xavier Roboam, *Member, IEEE*, and Luis Marroyo, *Member, IEEE*

***Abstract*—The use of doubly fed induction generators (DFIGs) in large wind turbines has become quite common over the last few years. These machines provide variable speed and are driven with a power converter which is sized for a small percentage of the turbine-rated power. A drawback of the DFIG is that it is very sensitive to grid disturbances, especially to voltage dips. However, the operation of the machine in these situations has only been studied in the literature by means of simulations. This paper develops a theoretical analysis of the dynamic behavior of the induction machine during three-phase voltage dips. The proposed analysis contributes to understanding the causes of the problem and represents a very useful tool to improve the existing solutions and propose new alternatives. Experimental results are in good agreement with those obtained theoretically and validate the proposed analysis.**

***Index Terms*—Doubly fed induction generator (DFIG), protection, wind power generation.**

NOMENCLATURE

$\vec{i}$	Current space vector.
L_m	Magnetizing inductance.
$L_{\rm ls}, L_{\rm lr}$	Stator and rotor leakage inductance.
L_s, L_r	Stator, rotor self-inductance.
r	Superscript denoting rotor reference frame.
R_s, R_r	Stator, rotor resistance.
s, r	Subscript denoting stator and rotor.
$\vec{v}$	Voltage space vector.
$\vec{\psi}$	Flux space vector.
$\omega_s, \omega_r, \omega$	Synchronous, slip and rotor angular frequency.

I. INTRODUCTION

WIND energy is now considered as an actual alternative to the conventional and pollutant energy sources such as oil, gas, and coal. Global wind power reached 47 GW in 2004 with a 20% growth in this year [1]. Due to their advantageous characteristics, most of the grid-connected wind turbines operate at a variable speed [2]. Among the different alternatives to obtain variable speed, the doubly fed induction generator (DFIG) is the most used. The basic configuration of a wind turbine based on a DFIG is shown in Fig. 1 [3].

Manuscript received September 29, 2005; revised March 3, 2006. This work was supported in part by the Spanish and the French Science and Education Ministries under Grant HF2004-0181. Paper no. TEC-00342-2005.

J. Lopez, P. Sanchis, and L. Marroyo are with the Department of Electrical and Electronic Engineering, Universidad Pública de Navarra, 31006 Pamplona, Spain (e-mail: jesus.lopez@unavarra.es; pablo.sanchis@unavarra.es; luisma@unavarra.es).

X. Roboam is with the Laboratoire d'Electrotechnique et d'Electronique Industrielle, INPT/CNRS, 31071 Toulouse Cedex 7, France (e-mail: xavier.roboam@leei.enseeiht.fr).

Digital Object Identifier 10.1109/TEC.2006.878241

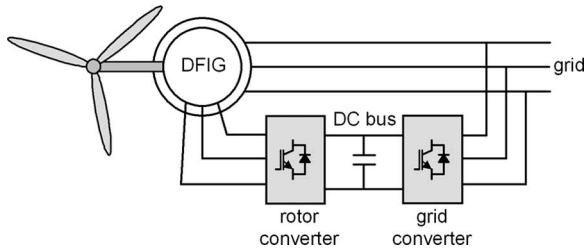

Fig. 1. Wind turbine scheme with DFIG.

As shown in the figure, the stator of the machine is directly connected to the grid, and only the rotor power must be handled by converters. Consequently, the control of the machine can be carried out with a converter that is sized for a power around 25%–35% of the rated power of the turbine. In addition to the common advantages in cost, size, and weight associated with a small converter, losses are also smaller compared to the system with a full power converter connected to the stator [4].

However, wind turbines based on the DFIG are very sensitive to grid disturbances, especially to voltage dips. The abrupt drop of the grid voltage causes overvoltages and overcurrents in the rotor windings that could even destroy the converter if no protection elements are included. Initially, the solution implemented by the manufacturers to protect the converter was to short circuit the rotor windings with the so-called crowbar and disconnect the turbine from the grid [5]. With this solution, the wind turbines are not able to collaborate in resuming normal operation of the grid. Even worse they contribute to increase the dip as they stop generating electric power. So far, the influence of the wind turbines on the evolution of the voltage dips has been small due to the low penetration of the wind energy. However, as the number of grid-connected turbines grows, this influence has become more important.

As an improvement on the crowbar, another solution proposes to connect resistances to the rotor. This way, the wind turbine can remain connected to the grid during the dips [6]. However, this solution is also not able to control the machine during the first moments of the dip. Additionally, sizing of the converter and resistances is made either experimentally or by simulation, and therefore it is quite difficult to optimize the system.

Recently, different studies have been proposed that try to predict the evolution of the electrical variables of the machine by means of simulation studies [6]–[10]. Based on simulations, these studies are unable to explain, from a theoretical viewpoint, the voltage dips that generate overcurrents as also the role played by each parameter in these situations. In some of these studies,

short explanations concerning the problem are provided that are sometimes even contradictory. For instance, [9] supposes that rotor overcurrents are caused by the instantaneous change of the stator flux. On the contrary, [6] gives a different explanation of the problem and considers that rotor overcurrents are due to the increase of the stator current caused by the voltage drop.

Simulations make it possible to predict the behavior of the machine but have obvious limitations. They are not useful to observe and isolate the influence of each parameter of the machine during the voltage dip. Therefore, they are usually not practical to propose and design possible solutions to avoid the consequences that voltage dips have on DFIGs.

In this context, a detailed theoretical analysis is necessary, describing the evolution of magnetic and electric variables of the generator during a voltage dip. Such an analysis can show, in particular, the influence of the system elements such as the machine parameters, the type of protection (crowbar), or the control of the generator. Finally, the behavior of the generator during a voltage dip has to be clearly analyzed, and the causes of the problem must be well understood.

This paper tries to help understand the dynamic behavior of the DFIG in the typical case of three-phase voltage dips. In the proposed analysis, the magnetic flux of the machine is divided into two components. The first component corresponds to the "forced flux" that rotates at synchronous speed and is related to the stator voltage. The second component is the "natural flux" that only appears during voltage transients. Unlike the forced flux, this natural flux does not rotate. As will be shown in the paper, the natural flux is the cause of the strong overvoltages in the rotor. If the rotor converter is not able to deal with these voltages, they will originate overcurrents in the stator and the rotor of the generator.

In this paper, simulation tests and experiments are proposed on a small machine rated at 3 kW. The objective is to provide a qualitative analysis of the system behavior during voltage dips. However, other simulation tests on large and representative DFIG, on the average of 1 MW reveal the phenomena to be qualitatively similar.

II. Generator Model

A model that is commonly used for the induction generator is the Park model [11]. For simplicity, the rotor variables will be referred to the stator. Although a synchronous rotating reference frame is often used, a static stator-oriented reference frame is more suitable for the purpose of this paper. Linear magnetic circuits are assumed. Using motor convention, the Park model can be expressed as

$$\vec{v}_s = R_s \cdot \vec{i}_s + \frac{d}{dt}\vec{\psi}_s \tag{1}$$

$$\vec{v}_r = R_r \cdot \vec{i}_r + \frac{d}{dt}\vec{\psi}_r - j\omega\vec{\psi}_r. \tag{2}$$

In a wind turbine, the stator is directly connected to the grid. That means that the stator voltage v_s is imposed by the grid. The rotor voltage v_r is controlled by a converter and is used to perform the machine control.

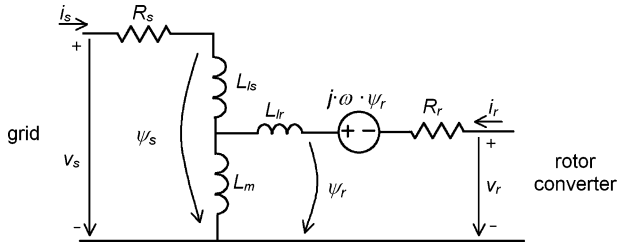

Fig. 2. Equivalent DFIG model.

The stator and rotor fluxes are given by

$$\vec{\psi}_s = L_s\vec{i}_s + L_m\vec{i}_r \tag{3}$$

$$\vec{\psi}_r = L_r\vec{i}_r + L_m\vec{i}_s. \tag{4}$$

Fig. 2 shows the equivalent electrical circuit corresponding to the previous equations.

From the converter viewpoint, the rotor voltage is one of the most important variable. This voltage is induced by the variation of the rotor flux, which can be calculated from (3) and (4)

$$\vec{\psi}_r = \frac{L_m}{L_s}\vec{\psi}_s - \sigma L_r \cdot \vec{i}_r. \tag{5}$$

From (2) and (5), the following expression is obtained:

$$\vec{v}_r = \frac{L_m}{L_s}\left(\frac{d}{dt} - j\omega\right)\vec{\psi}_s + \left(R_r + \sigma L_r\left(\frac{d}{dt} - j\omega\right)\right)\vec{i}_r. \tag{6}$$

The rotor voltage given by (6) can be divided into two terms. The first one is denoted voltage v_{r0} and is due to the stator flux. It is the rotor voltage when the rotor is in an open-circuit condition ($i_r = 0$). Its expression is therefore

$$\vec{v}_{r0} = \frac{L_m}{L_s}\left(\frac{d}{dt} - j\omega\right)\vec{\psi}_s. \tag{7}$$

The second term only appears if there is current in the rotor. It is due to the voltage drop in both the rotor resistance R_r and the rotor transient inductance σL_r.

III. Normal Operation

In normal operation, the stator voltage space phasor is a rotating vector of constant amplitude V_s that rotates at synchronous speed ω_s

$$\vec{v}_s = V_s e^{j\omega_s t}. \tag{8}$$

If the resistance R_s is neglected, the expression for the stator flux can be obtained from (1) and (8)

$$\vec{\psi}_s = \frac{V_s}{j\omega_s}e^{j\omega_s t} = \vec{\Psi}_{\mathrm{sf}} \cdot e^{j\omega_s t}. \tag{9}$$

At steady state, the stator flux is a vector whose amplitude is constant and proportional to the grid voltage. This vector rotates at synchronous frequency and represents the forced response of the system. Therefore, this term can be called stator forced flux (ψ_{sf}).

By substituting (9) in (7), the term of the rotor voltage due to the stator flux is

$$\vec{v}_{r0} = j\omega_r \frac{L_m}{L_s}\vec{\psi}_s = \frac{L_m}{L_s}\frac{\omega_r}{\omega_s}V_s e^{j\omega_s t} \tag{10}$$

where $\omega_r = \omega_s - \omega$.

The rotor voltage due to the stator flux is proportional to the slip frequency. For instance, if the rotor rotates at synchronous speed, the windings see a constant flux and then the induced voltage is zero. In any other situation, the rotor voltage depends on the difference between the synchronous and the rotor speed. The amplitude of the voltage v_{r0} can be expressed as a function of the amplitude of the stator voltage

$$V_{r0} = V_s \frac{L_m}{L_s}\frac{\omega_r}{\omega_s} = V_s \frac{L_m}{L_s} s \tag{11}$$

where s is the slip ($s = \omega_r/\omega_s$).

Previous equations describe the rotor voltage when there is no rotor current. However, in normal operation, the rotor converter controls the rotor current in order to achieve the reference active and reactive powers. The voltage at rotor terminals that has to be generated by the converter is

$$\vec{v}_r = \vec{v}_s \frac{L_m}{L_s} s + \left(R_r + \sigma L_r \left(\frac{d}{dt} - j\omega\right)\right)\vec{i}_r. \tag{12}$$

The rotor resistance and the transient inductance ($\sigma.L_r$) are often very small. In addition, rotor currents also have a small frequency (ω_r<10 Hz). As a consequence, the voltage at rotor terminals does not differ substantially from v_{r0}.

IV. Behavior of the Machine Under a Full-Voltage Dip

This section analyzes the behavior of the generator during a full-voltage dip. The analysis is particularly for an instantaneous voltage dip. Obviously, this is not possible in real systems. In these systems, the voltage drops with a particular derivative that depends on the grid and the characteristics of the fault that has generated the voltage dip. There are two reasons why an instantaneous voltage dip has been considered.

1) It is the worst situation. In any other situation, the voltages induced in the rotor are lower.
2) In regulation codes, a time of 1 ms is usually established for the voltage to drop. The difference between this abrupt voltage dip and an instantaneous voltage dip is negligible. Differences in the induced rotor voltage during both kinds of dips are lower than 1%.

The generator operates at normal condition when, at time $t = t_0$, a fault appears in the grid. This fault can be caused, for instance, by a near short circuit. The stator voltage is

$$\begin{aligned} \vec{v}_s(t{<}t_0) &= V_s e^{j\omega_s t} \\ \vec{v}_s(t \geq t_0) &= 0. \end{aligned} \tag{13}$$

Therefore, the steady-state stator flux, i.e., the forced flux, before and during the voltage dip is

$$\begin{aligned} \vec{\psi}_{\rm sf}(t{<}t_0) &= \frac{V_s}{j\omega_s} e^{j\omega_s t} \\ \vec{\psi}_{\rm sf}(t \geq t_0) &= 0. \end{aligned} \tag{14}$$

However, the flux cannot be discontinuous because it is a state variable. Therefore, it cannot cancel instantaneously. On the contrary, the flux in the machine evolves from its initial value to zero. This transient evolution of the stator flux implies a transient evolution of the term v_{r0} of the rotor voltage.

As a first step, the situation in which the rotor is in an open-circuit condition is previously analyzed. After that, the influence of the rotor current is included in the analysis.

A. Open-Circuit Rotor

In this situation, rotor currents are zero and the rotor voltage is just v_{r0}. The expression for the stator flux is obtained from (1) and (3)

$$\frac{d}{dt}\vec{\psi}_s = \vec{v}_s - \frac{R_s}{L_s}\vec{\psi}_s. \tag{15}$$

The solution of (15) for $t \geq t_0$ can be divided into two parts. The first one corresponds to the forced flux, or steady-state flux. According to (9), this flux is proportional to the grid voltage, being therefore zero in this case. The second term corresponds to the natural flux, $\psi_{\rm sn}$. This flux does not depend on the voltage but only depends on the magnetic state of the machine. The natural flux is a transient flux that guarantees that no discontinuities appear in the magnetic state of the machine when it changes its point of operation. In short, the stator flux corresponds with the natural flux during the voltage dip. The evolution of the stator flux is obtained from (15) if $t_0 = 0$ is assumed

$$\begin{aligned} \vec{\psi}_s(t{<}t_0) &= \vec{\psi}_{\rm sf} = \frac{V_s}{j\omega_{\rm s}} e^{j\omega_s t} \\ \vec{\psi}_s(t \geq t_0) &= \vec{\psi}_{\rm sn} = \frac{V_s}{j\omega_s} e^{j\omega_s t_0} e^{-tR_s/L_s} = \vec{\Psi}_0 \cdot e^{-t/\tau_s} \end{aligned} \tag{16}$$

where V_s and Ψ_0 are the stator voltage and flux, respectively, just before the voltage dip.

The natural flux that appears when the voltage dip occurs is a fixed vector with respect to the stator. Its amplitude decreases exponentially to zero according to the time constant of the stator. Fig. 3 shows the trajectory of the spatial vector of the stator flux, which is obtained from (16), for the generator described in the Appendix.

By means of (3) and (16), and taking into account that the rotor is in an open-circuit condition, the stator current is obtained

$$\begin{aligned} \vec{i}_s(t{<}t_0) &= \frac{\vec{\psi}_s(t{<}t_0)}{L_s} = \frac{V_s}{j\omega_s L_s} e^{j\omega_s t} \\ \vec{i}_s(t \geq t_0) &= \frac{\vec{\psi}_s(t \geq t_0)}{L_s} = \frac{\vec{\Psi}_0 \cdot e^{-t/\tau_s}}{L_s}. \end{aligned} \tag{17}$$

Fig. 4 shows the evolution of the stator currents for the generator described in the Appendix. As shown, the natural flux causes a dc current that flows through the stator. The amplitude of this current decreases exponentially. The initial amplitude of the current of each phase corresponds to its instantaneous value at the time the voltage dip appears. As the generator is small, the time constant of the stator is $\tau_s = 100$ ms, and therefore

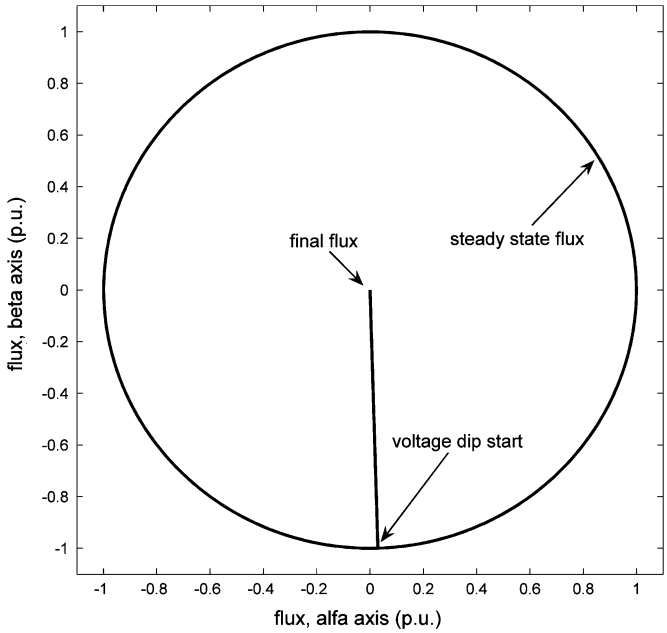

Fig. 3. Stator flux trajectory.

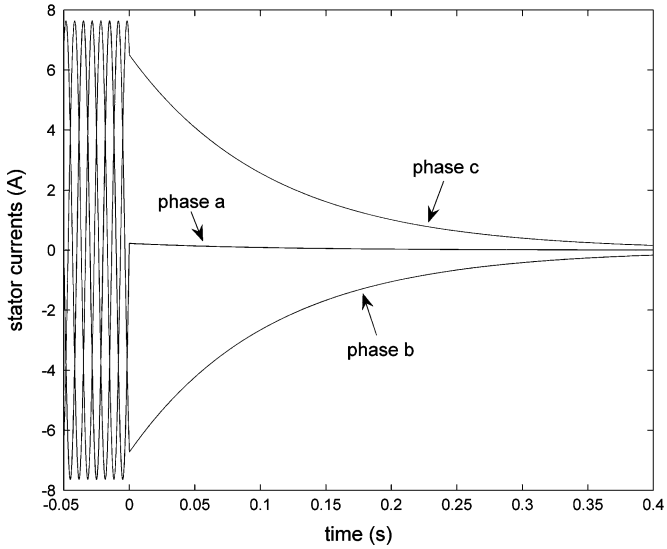

Fig. 4. Stator currents.

the transient lasts around 300 ms. In larger generators, this time constant is quite bigger, up to 1–1.5 s for generators of 1 MW. In these cases, the transient can last some seconds.

By substituting (16) in (7), the induced voltage in the rotor during the dip is obtained

$$\vec{v}_{r0} = -\frac{L_m}{L_s}\left(\frac{1}{\tau_s} + j\omega\right) \cdot \vec{\Psi}_0 \cdot e^{-t/\tau_s}. \tag{18}$$

This voltage is a space vector that is fixed to the stator. Its amplitude decreases exponentially to zero. With respect to the rotor windings, this voltage rotates reversely

$$\vec{v}_{r0}{}^{r} = -\frac{L_m}{L_s}\left(\frac{1}{\tau_s} + j\omega\right) \cdot \vec{\Psi}_0 \cdot e^{-t/\tau_s} e^{-j\omega t}. \tag{19}$$

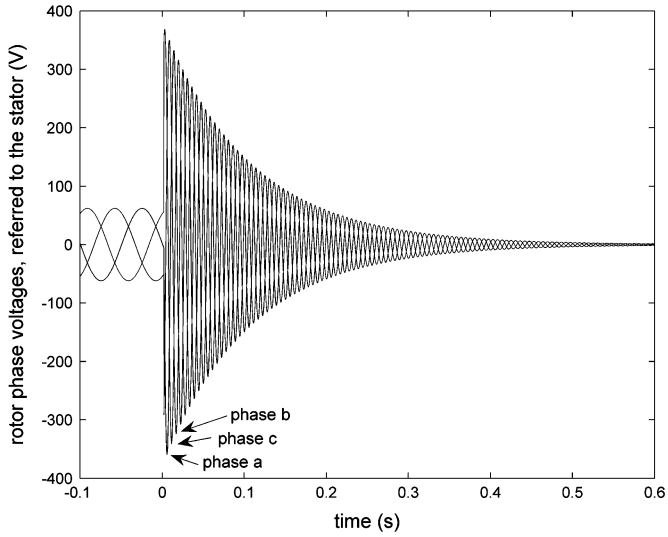

Fig. 5. Rotor voltages with $s = -0.2$.

Fig. 5 shows the rotor voltages with a slip of -20%. The amplitude of v_{r0} achieves its maximum value at the moment of the voltage dip. Using (19) and neglecting the term $1/\tau_s$ due to its low value, this amplitude is obtained

$$V_{r0}(t_0) \approx \frac{L_m}{L_s}\frac{\omega}{\omega_s}V_s = \frac{L_m}{L_s}(1-s)V_s. \tag{20}$$

According to (20), V_{r0} is proportional to $1 - s$. On the contrary, the steady-state voltage is proportional to s, as given by (11). Since the slip is usually constrained to a range between -0.2 and 0.2, it can be concluded that the amplitude of the voltage induced in the rotor at the first moment of the dip is similar to the stator rated voltage instead of the small percentage induced in normal operation. It can even be higher if the machine operates at super-synchronous speed.

B. Rotor Connected to the Converter

When there are currents flowing into the rotor, they affect the voltage according to (6)

$$\vec{v}_r = \vec{v}_{r0} + \left(R_r + \sigma L_r\left(\frac{d}{dt} - j\omega\right)\right)\vec{i}_r. \tag{21}$$

The rotor voltage in (21) can be expressed in a rotor reference frame

$$\vec{v}_r{}^{r} = \vec{v}_{r0}\, e^{-j\omega t} + R_r \cdot \vec{i}_r^{\,r} + \sigma L_r \frac{d\vec{i}_r^{\,r}}{dt}. \tag{22}$$

From the last expression, the equivalent circuit of the machine from the viewpoint of the rotor can be obtained as shown in Fig. 6.

From the viewpoint of the rotor, the machine behaves as a voltage supply in series with the transient inductance σL_r and the rotor resistance R_r. The voltage supply represents the voltage due to the stator flux. In order to avoid losing the control of the current, the converter should be sized to be able to generate a voltage equal to the maximum voltage of the supply, as stated

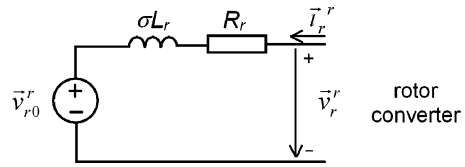

Fig. 6. Machine model from the viewpoint of the rotor.

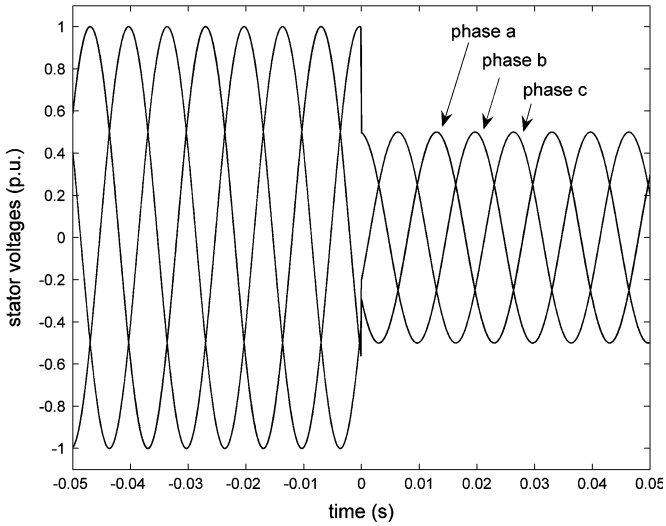

Fig. 7. Grid phase voltages for a 50% dip.

in (20). That means a voltage similar to the stator-rated voltage. However, that would imply a converter with a rated power similar to that of the generator, losing therefore the advantages of this power conversion structure.

If the converter is sized for a voltage lower than V_{r0}, the rotor current will remain uncontrolled transitorily. The overcurrent will depend on both the maximum value of the voltage that can generate the converter and the rotor transient inductance σL_r and resistance R_r. These elements often have a small value, and therefore high overcurrents are likely to appear. According to the machine model proposed in Fig. 6, it becomes clear that limiting these overcurrents requires us to oversize the converter or connect external impedances. With this analytical model, the impedances can be calculated so as to limit the rotor current up to a desired value.

V. Behavior Under a Partial-Voltage Dip

This section analyzes the influence of the depth of the voltage dip on the rotor-induced voltage. The generator is assumed to be operating in normal condition when, at a given moment $t = t_0$, the voltage amplitude brutally changes from V_1 to V_2

$$\vec{v}_s = \begin{cases} V_s e^{j\omega_s t} = V_1 e^{j\omega_s t} & \text{for } t<t_0 \\ V_2 e^{j\omega_s t} & \text{for } t \geq t_0 \end{cases}. \tag{23}$$

As an example, Fig. 7 shows the evolution of the stator voltages for a 50% dip.

Fig. 8. Decomposition of the flux at the beginning of the dip.

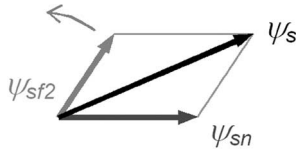

Fig. 9. Evolution of the flux during the voltage dip.

The steady-state stator flux, i.e., the forced flux, is proportional to the voltage

$$\vec{\psi}_{\rm sf} = \begin{cases} \vec{\psi}_{\rm sf1} = \frac{V_1}{j\omega_s} e^{j\omega_s t} & \text{for } t<t_0 \\ \vec{\psi}_{\rm sf2} = \frac{V_2}{j\omega_s} e^{j\omega_s t} & \text{for } t \geq t_0 \end{cases}. \tag{24}$$

The flux being a state variable, it cannot have discontinuities. It means that it cannot change from $\Psi_{\rm sf1}$ to $\Psi_{\rm sf2}$ instantaneously. On the contrary, the flux changes progressively. As a consequence, a natural flux appears again in order to guarantee that no discontinuity happens in the flux. This natural flux induces important voltages in the rotor.

Similar to the previous section, the rotor open-circuit condition is first analyzed.

A. Open-Circuit Rotor

Assuming $t_0 = 0$ and from (15) and (24), the following expression is obtained

$$\vec{\psi}_{\rm s}(t) = \vec{\psi}_{\rm sf2} + \vec{\psi}_{\rm sn} = \frac{V_2}{j\omega_s} e^{j\omega_s t} + \frac{V_1 - V_2}{j\omega_s} e^{-t/\tau_s}. \tag{25}$$

The last expression shows that the stator flux consists of a rotational term that is determined by the grid voltage, and a term with a constant argument due to the natural mode. Fig. 8 shows the flux decomposition just before and after the dip appears. Fig. 9 shows the decomposition during the dip.

Due to the forced flux, the stator flux spatial vector tracks a circle, and due to the natural flux this circle is not centered. Fig. 10 shows the trajectory of the flux for a 50% dip. Before the dip, the flux tracks a circle with a per unit radius that is equal to 1.

When the dip appears, the size of the circle decreases as the voltage reduces, and moves as a consequence of the natural flux. During the dip, the circle moves to the center as the natural flux goes to zero. After the transitory finishes, the steady-state natural flux disappears and the trajectory of the flux is centered again.

Each of the two components of the flux induces a corresponding component in the open-circuit rotor voltage v_{r0}. The first component is induced by the forced flux and the second one is created by the natural flux

$$\vec{v}_{r0} = \vec{v}_{\rm rf} + \vec{v}_{\rm rn}. \tag{26}$$

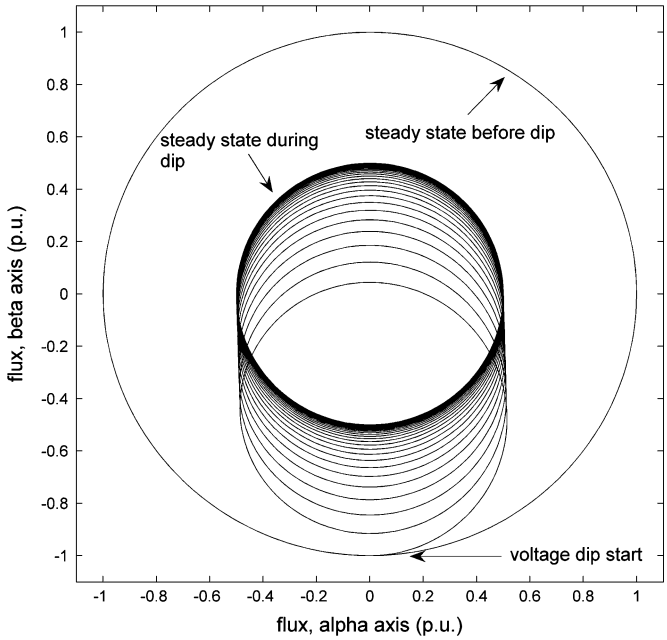

Fig. 10. Stator flux trajectory for a 50% voltage dip.

From t_0, the voltage induced by the forced flux is proportional to the stator voltage V_2 and the slip

$$\vec{v}_{\rm rf} = V_2 \frac{L_m}{L_s} s e^{j\omega_s t}. \tag{27}$$

By substituting in (7) the flux by the natural flux shown in (25), the following expression is achieved:

$$\vec{v}_{\rm rn} = -\frac{L_m}{L_s}\left(\frac{1}{\tau_s} + j\omega\right)\frac{V_1 - V_2}{j\omega_s} e^{-t/\tau_s}. \tag{28}$$

If the term $1/\tau_s$ is neglected, (28) reduces to

$$\vec{v}_{\rm rn} \approx -\frac{L_m}{L_s}\frac{\omega}{\omega_s}(V_1 - V_2)\, e^{-t/\tau_s}. \tag{29}$$

The two components $v_{\rm rf}$ and $v_{\rm rn}$ can now be added and the result can be expressed in a rotor reference frame

$$\vec{v}_{r0}^{\,r} \approx \frac{L_m}{L_s}\left(sV_2 e^{j\omega_r t} - (1-s)(V_1 - V_2) e^{-j\omega t} e^{-\frac{t}{\tau_s}}\right). \tag{30}$$

The two terms of the previous equation are different in nature. The first one is generated by the new grid voltage and its amplitude is small as it is proportional to the slip. Its frequency is the difference between the synchronous and the rotor frequencies; therefore, it usually achieves some Hertz. The second voltage is a transient term caused by the natural flux. Its amplitude can be important as it is proportional to the depth of the dip $(V_1 - V_2)$. In addition, its frequency is the rotor electrical speed ω.

The maximum amplitude of the rotor voltage v_{r0} appears at $t = 0$ in supersynchronous operation and at half the grid period ($t = 10$ ms for 50 Hz) in subsynchronous operation. Its value is the sum of the amplitude of the two voltages

$$V_{r0,\max} \approx \frac{L_m}{L_s}(|s|V_2 + (1-s)(V_1 - V_2)). \tag{31}$$

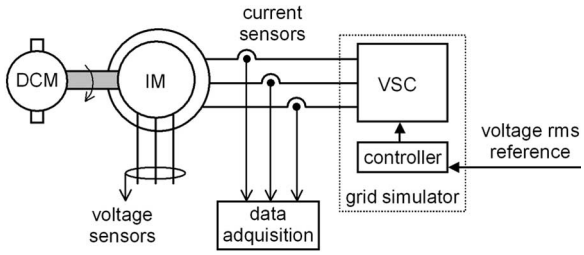

Fig. 11. Experimental setup.

B. Rotor Connected to the Converter

If the depth of the dip is small and the voltage induced by the stator flux does not exceed the maximum voltage that the rotor converter can generate, the current remains controlled. In this case, as in the normal operation, the voltage at rotor terminals does not vary substantially from the value obtained in (31). Therefore, this expression can be used to calculate the maximum dip depth that the DFIG can hold.

For larger dips, the voltage induced by the stator flux exceeds the maximum available tension of the converter and the control of the current is lost transitorily. In this situation, there appear overcurrents that increase as the depth of the dip is bigger. The worst case is the one corresponding to the full dip, which has been previously analyzed.

In fact, the rotor converter power rating is quite proportional to the accepted rate of the dip depth.

VI. Experimental Results

In order to validate the results obtained in the previous sections, several experimental tests were performed using the system whose block diagram is shown in Fig. 11.

The experimental setup includes the following items.

1) A 3-kW wound rotor induction machine whose data are listed in the Appendix. The rotor was open circuited.
2) A dc motor driving the machine at constant speed.
3) The stator was connected to a voltage source converter (VSC) operating at a 10-kHz switching frequency. This converter was controlled to simulate voltages dips. It provides a balanced three-phase voltage system with variable amplitude.
4) The rotor voltages and the stator currents were measured by LEM sensors. Analog filters with a cutoff frequency of 2 KHz have been adopted in order to filter the switching harmonics of the VSC.

A. Behavior Under a Full Dip, Supersynchronous Speed

The DFIG was first tested under a full-voltage dip that appears at $t_0 = 0$ s when the machine operated 20% above the synchronous speed ($s = -0.2$). Fig. 12 shows the evolution of the measured stator currents. It can be observed that currents continue flowing even when the voltage is zero. This fact proves that the machine is still magnetized. As was obtained in the analysis of Section V, currents are continuous and their amplitude

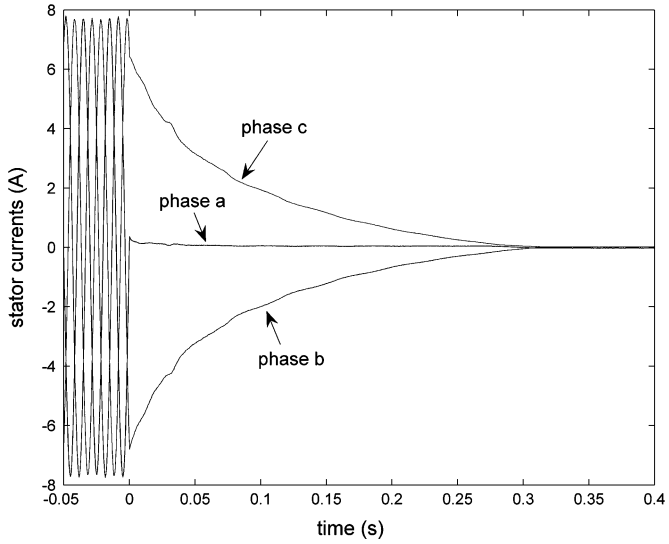

Fig. 12. Experimental stator phase currents in a total dip.

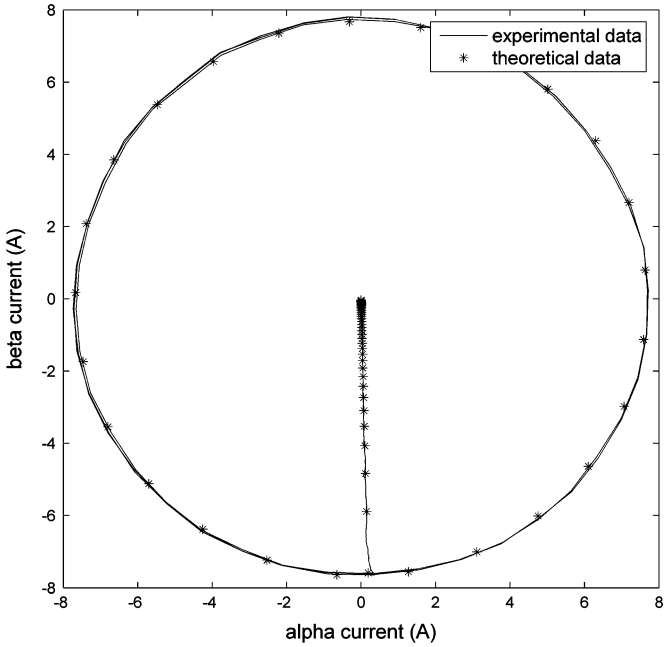

Fig. 13. Theoretical and experimental trajectories of the stator current during a full dip.

decreases exponentially. The shape of the waveform is similar to the one shown in Fig. 4, which was obtained theoretically.

Because the rotor is in an open-circuit condition, the flux is proportional to the stator current. The tracking of the flux spatial phasor is then similar to the current phasor. Fig. 13 shows the current phasor when it is experimentally measured, together with the current phasor obtained theoretically by means of (17). Both theoretical and experimental results are in good agreement. In both cases, the flux tracks a circular trajectory before the dip. When the voltage decreases, the flux stops rotating and it remains with the same argument while its amplitude decreases as the machine demagnetizes. This flux, which exists even when the stator voltage is zero, is the natural flux that was analyzed in the previous sections. Because this flux is stopped with respect to the stator, important voltages are induced in the rotor.

Fig. 14 shows the rotor phase voltages. The measured waveforms are similar to those that were obtained theoretically and shown in Fig. 5. Before the dip, the rotor voltages correspond to the normal operation with $s = -0.02$. Their peak value achieves around 40 V. When the full dip appears, the natural flux induces voltages whose amplitude evolves in the same way as the stator flux (or current), i.e., they decrease exponentially. The analysis of the three-phase voltages shows that their frequency equals the rotor frequency, 60 Hz, and that they are in negative sequence.

From Fig. 14, the peak value of the phase voltage when the full dip appears achieves 210 V. In order to validate the theoretical analysis developed in the previous sections, the experimental value can be compared with the theoretical one obtained according to (20). As the root-mean-square-value of the stator line-to-line voltage before the dip is 380 V, the rotor voltage results are

$$V_s = 311 \text{ V}$$
$$V_{r0}(0) \approx \frac{L_m}{L_s}(1-s)V_s = 366.8 \text{ V}. \tag{32}$$

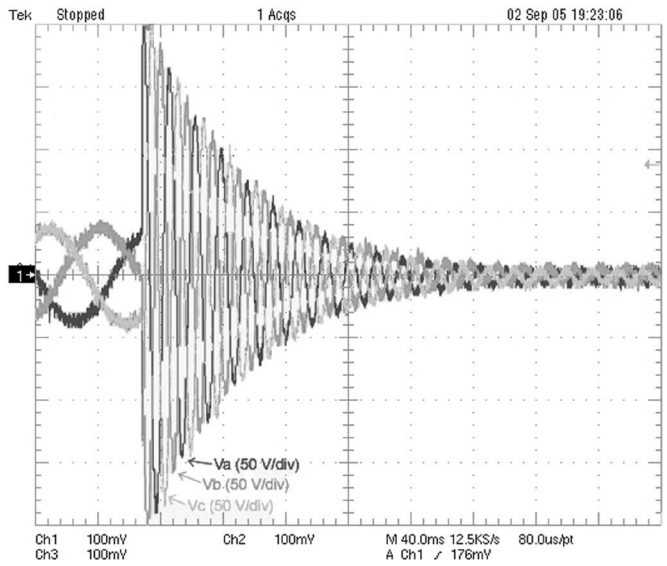

Fig. 14. Rotor phase voltages during a full dip.

Now, this voltage is referred to the rotor, regarding the transformation ratio (0.613)

$$V'_{r0} = V_{r0} \times 0.613 = 224.8 \text{ V}. \tag{33}$$

As can be seen, experimental and theoretical values are in good agreement.

B. Behavior Under a 50% Dip, Supersynchronous Speed

The trajectory of the stator current phasor (proportional to the flux vector) during a 50% dip is shown in Fig. 15. This figure also presents the current calculated from the flux obtained in (24) and (25). In order to achieve a higher accuracy, the magnetizing

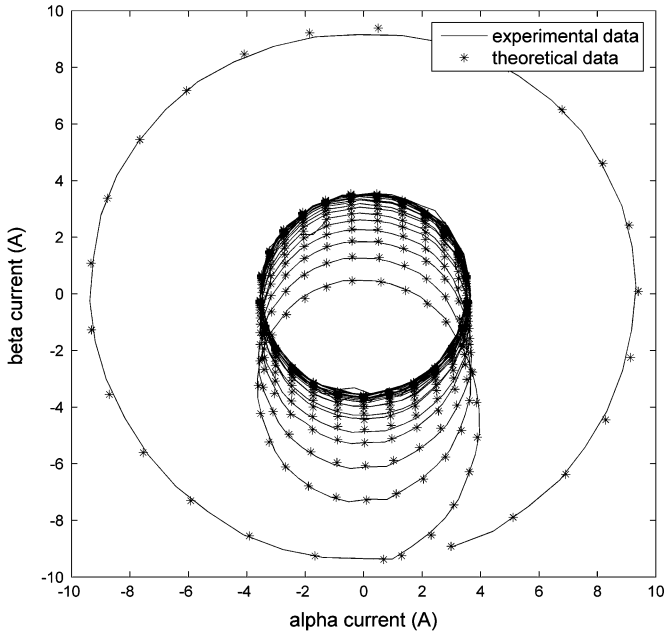

Fig. 15. Experimental and theoretical trajectory of the stator current during a 50% dip.

curve of the machine has also been considered. This curve is given in the Appendix together with the machine parameters. As described in Section V, the trajectory can be explained by splitting the flux into two terms, the natural and forced fluxes. The first one is caused by the voltage and has a circular trajectory whose diameters are approximately equal to half the diameter of the circle before the dip. The second one guarantees that the flux does not have any discontinuity. Its argument is constant and causes the flux trajectory to be not centered. As long as the natural flux disappears, the trajectory moves to the center until it centers completely at steady state.

The voltage induced in the rotor windings during this test is shown in Fig. 16. The shape of the voltage waveforms is very similar to the one of a full dip (see Fig. 14) except for the fact that the voltage is now the sum of the voltage induced by the forced flux, with a frequency of 10 Hz, and the voltage induced by the natural flux, whose frequency is 60 Hz.

The maximum amplitude of the voltages shown in Fig. 16 is 125 V. According to (31), the theoretical value of this amplitude is

$$\begin{aligned} V_1 &= 311 \text{ V} \\ V_2 &= 155.5 \text{ V} \\ V_{r0}(0) &\approx \frac{L_m}{L_s}(|s|V_2 + (1-s)(V_1 - V_2)) = 214 \text{ V}. \end{aligned} \tag{34}$$

Now, referring this voltage to the rotor

$$V'_{r0} = V_{r0} \times 0.613 = 131.2 \text{ V}. \tag{35}$$

Again, experimental results agree with those predicted by the theoretical analysis.

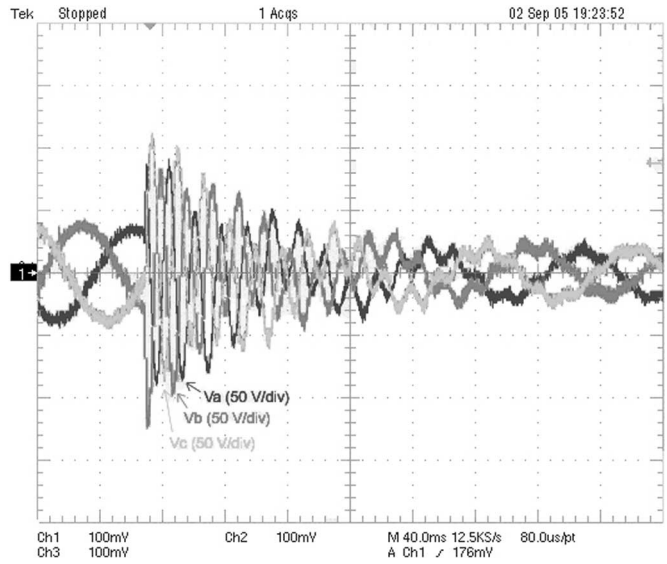

Fig. 16. Rotor phase voltages in a 50% dip.

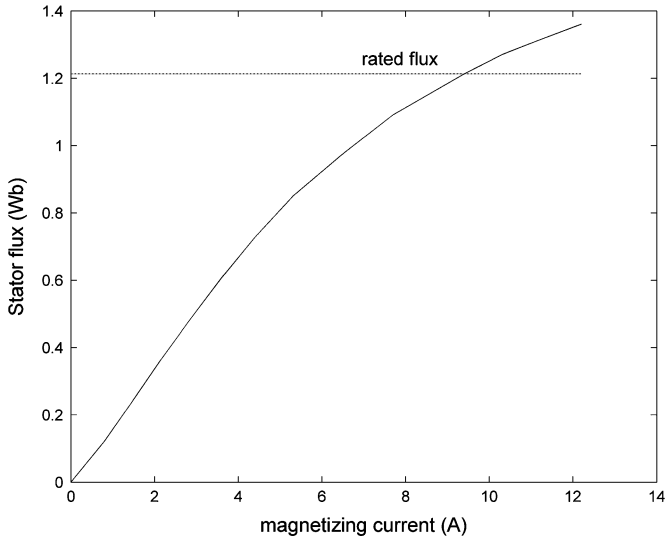

Fig. 17. Generator open-circuit curve.

VII. Conclusion

A theoretical analysis of the behavior of the DFIG during full- or partial-voltage dips has been proposed. In this analysis, the stator flux is divided into two components, the natural and the forced flux. The forced flux, which rotates at synchronous speed, appears during the normal operation of the machine. It induces a voltage in the rotor proportional to the slip. As the machine typically operates with slips up to 20%, this voltage is relatively low. The natural flux is a transient flux that appears during the voltage dips. Its initial value is proportional to the voltage change and decays exponentially according to the stator time constant. Unlike the forced flux, it remains fixed to the stator, and therefore it is seen by the rotor as a flux that rotates at the rotor speed. As a consequence, the natural flux induces voltages in the rotor that are much greater than those appearing at steady state. In the case of strong voltage dips, the induced

voltage at supersynchronous speed can even be higher than the stator voltage. If the rotor converter does not compensate this overvoltage, the control of the current is lost transitorily. In this situation, there appear overcurrents whose amplitude depends on the depth of the dip, the maximum voltage of the converter, the machine parameters, and the protection elements.

The paper proposes a rigorous approach to these complex transient phenomena in order to analyze the dynamic behavior of a doubly fed induction machine during a voltage dip. The analysis is, in particular, for an instantaneous voltage dip, which is representative of the abrupt voltage dips that usually appear in real situations. It opens interesting prospects toward the search of hardware and software solutions allowing to face the grid interactions of DFIG-based wind power systems.

APPENDIX

TABLE I
GENERATOR DATA

Rated power:	3 kW
Rated stator voltage:	$U_n = 380$ V
Rated frequency:	50 Hz
Stator resistance:	$R_s = 1.2\ \Omega$
Mutual inductance:	$L_m = 0.127$ H
Stator leakage inductance:	$L_{ls} = 0.0022$ H
Number of pole pairs:	pn = 2
Transformation ratio:	0.613

REFERENCES

[1] "Global wind power continues expansion," press note by GWEC, Brussels, Mar. 2004, [Online]. Available: www.gwec.net/index.php?id=30&tx_ttnews%5Btt_news%5D=1

[2] H. L. Nakra and B. Duke, "Slip power recovery induction generators for large vertical axis wind turbines," *IEEE Trans. Energy Convers.*, vol. 3, no. 4, pp. 733–737, Dec. 1988.

[3] R. Pena, J. C. Clare, and G. M. Asher, "Doubly fed induction generator using back-to-back PWM converters and its application to variable speed wind-energy generation," *Proc. Inst. Electr. Eng. Electr. Power Appl.*, vol. 143, no. 3, pp. 231–241, May 1996.

[4] A. Petersson and S. Lundberg, "Energy efficiency comparison of electrical systems for wind turbines," presented at the IEEE Nordic Workshop Power Industrial Electron. (NORpie/2002), Stockholm, Sweden, 2002.

[5] N. Jouko, "Voltage dip ride through of a double-fed generator equipped with an active crowbar," presented at the Nordic Wind Power Conference, Chalmers University of technology, Gothenburg, Sweden, Mar. 2004.

[6] T. Thiringer, A. Petersson, and T. Petru, "Grid disturbance response of wind turbines equipped with induction generator and doubly-fed induction generator," in *Proc. IEEE Power Eng. Soc. Gen. Meeting*, 2003, vol. 3, pp. 1542–1547.

[7] A. Perdana, O. Carlson, and J. Persson, "Dynamic response of grid-connected wind turbine with doubly fed induction generator during disturbances," presented at the Nordic Workshop Power Industrial Electron., Trondheim, Norway, 2004.

[8] T. Sun, Z. Chen, and F. Blaabjerg, "Transient analysis of grid-connected wind turbines with DFIG after an external short-circuit fault," presented at the Nordic Wind Power Conf., Chalmers Univ. Technol., Gothenburg, Sweden, Mar. 2004.

[9] J. B. Ekanayake, L. Holdsworth, X. G. Wu, and N. Jenkins, "Dynamic modeling of doubly fed induction generator wind turbines," *IEEE Trans. Power Electron.*, vol. 18, no. 2, pp. 803–809, May 2003.

[10] J. Morren and S. W. H. de Haan, "Ridethrough of wind turbines with doubly-fed induction generator during a voltage dip," *IEEE Trans. Energy Convers.*, vol. 20, no. 2, pp. 435–441, Jun. 2005.

[11] W. Leonhard, *Control of Electrical Drives*. Berlin: Springer-Verlag, 1995.

Jesús López (M'05) was born in Pamplona, Spain, in 1975. He received the M.Sc. degree in industrial engineering from the Public University of Navarra, Pamplona, in 2000. Currently, he is working toward the Ph.D. degree at the Department of Electrical and Electronic Engineering, Public University of Navarra in collaboration with the Laboratory of Electrotechnics and Industrial Electronics, Toulouse, France.

In 2001, he joined the Power Electronic Group, Electrical and Electronic Department, Public University of Navarra, where he is currently an Assistant Professor and is also involved in research projects mainly in cooperation with the industry. His current research interests include the field of power electronics, power systems quality, and renewable energies, such as wind and photovoltaic plants.

Pablo Sanchis (M'03) received the M.Sc. and the Ph.D. degrees in electrical engineering, in 1995 and 2002, respectively, from the Public University of Navarra, Pamplona, Spain, and the M.Sc. degree in management and business administration in 1994, also from the Public University of Navarra.

From 1996 to 1998, he worked as a Guest Researcher at Delft University of Technology, Delft, The Netherlands, in the field of control of electrical machines. Since 1998, he is an Assistant Professor at the Department of Electrical and Electronic Engineering at the Public University of Navarra, where he is engaged in many research projects mainly in cooperation with the industry. His current research interests include power electronics, distributed generation, control of power converters, photovoltaic and hybrid systems, alternative energy systems, and hydrogen generation from renewable sources.

Xavier Roboam (M'96) received the Ph.D. degree in electrical engineering from the Institut National Polytechnique de Toulouse, Toulouse, France, in 1991.

Since 1992, he has been a Full-Time Researcher in the Laboratory of Electrotechnics and Industrial Electronics of Toulouse. Since 1998, he is the Head of the team "System" whose objective is to process the design problem in electrical engineering at a "system level." He is engaged in developing methodologies specifically oriented toward multifields systems design for applications such as electrical embedded systems or renewable energy systems.

Luis Marroyo (M'03) received the M.Sc. degree in electrical engineering in 1993 from the University of Tolouse, Toulose, France, and the Ph.D. degree in electrical engineering, in 1997 from the Public University of Navarra, Pamplona, Spain, and in 1999 from the Laboratory of Electrotechnics and Industrial Electronics-École Nationale Supériere of Electrical Engineering, Electronics, Data Processing, Hydraulics, and Telecommunication Institut National Polytechnique de Toulouse, Toulouse, France.

From 1993 to 1998, he was an Assistant Professor at the Department of Electrical and Electronic Engineering of the Public University of Navarra, where he is currently an Associate Professor since 1998. His current research interests include power electronics, grid quality, and renewable energy.